

Seismic and geodetic investigation of the 1996–1998 earthquake swarm at Strandline Lake, Alaska

Wayne W. Kilgore,¹ Diana C. Roman,^{1*} Juliet Biggs^{2†} and Roger Hansen³

¹Department of Geology, University of South Florida, Tampa, FL, USA. E-mail: droman@usf.edu

²Rosenstiel School of Marine and Atmospheric Sciences, University of Miami, Miami, FL, USA

³Alaska Earthquake Information Center, University of Alaska Fairbanks, Fairbanks, AK, USA

Accepted 2011 June 14. Received 2011 June 10; in original form 2010 July 15

SUMMARY

Microearthquake swarms occur frequently in volcanic environments, but do not always culminate in an eruption. Such non-eruptive swarms may be caused by stresses induced by magma intrusion, hydrothermal fluid circulation or possibly other tectonic processes such as slow-slip earthquakes. The Strandline Lake region of southcentral Alaska, located 30 km northeast of Mt Spurr volcano, experienced an intense earthquake swarm between 1996 August and 1998 September. A total of 2507 earthquakes were recorded by the Alaska Volcano Observatory's permanent seismic network during the swarm period, with a maximum magnitude of M_L 3.6. The cumulative seismic moment of the swarm was 1.2×10^{15} N m, equivalent to that of a single M_w 4.0 earthquake. Because of the swarm's distance from the nearest Holocene volcanic vent, seismic monitoring was minimal and gas emission and GPS data do not exist for the swarm period. However, combined waveforms from a dense seismic network on Mt Spurr and from several regional seismic stations allow reanalysis of a representative set of swarm and background earthquakes. Swarm hypocentres calculated using a newly formulated 1-D velocity model and station corrections indicate a roughly circular swarm volume with dimensions of approximately 5 km, centred below 10 km below sea level (BSL). Composite fault-plane solutions for swarm earthquakes indicate oblique strike-slip faulting with a northeast-trending P -axis orientation. In contrast, a composite fault-plane solution for background earthquakes indicates a fundamentally different, though poorly constrained, local stress field orientation. Interferometric Synthetic Aperture Radar images spanning the swarm period unambiguously show no evidence of surface deformation, but do not rule out subcentimetre-scale deformation during the swarm. While a shallow (<10 km BSL) magma intrusion appears to be an unlikely cause of the 1996–1998 Strandline Lake swarm based on the new earthquake depths and the absence of strong surface deformation, it is possible that the swarm was driven by deep (>10 km BSL) magma intrusion representing an intrusive or protovolcanic segment of the Aleutian arc.

Key words: Radar interferometry; Earthquake source observations; Seismicity and tectonics; Volcano seismology; Volcanic arc processes; Dynamics and mechanics of faulting.

1 INTRODUCTION AND BACKGROUND

Intense swarms of low-magnitude earthquakes are a common phenomenon in volcanically and tectonically active regions (e.g. Vidale *et al.* 2006). Earthquake swarms are spatiotemporally clustered sequences of earthquakes in which there is no principal event, distinguishing them from main shock–aftershock sequences

(Yamashita 1998). The largest earthquake in a swarm typically occurs in the middle of the sequence and the spatial distribution of swarm hypocentres may be random within a small cloud-like volume (e.g. Benoit & McNutt 1996). Some earthquake swarms are clearly driven by magmatic processes, as they are followed by an eruption (e.g. Umakoshi *et al.* 2001) or accompanied by other indications of magma ascent such as increased gas emissions (e.g. Roman *et al.* 2004) or surface deformation (e.g. Lu *et al.* 2000). Other earthquake swarms, including those related to induced fluid circulation (e.g. Ake *et al.* 2005; Häring *et al.* 2008; Dorbath *et al.* 2010; Horalek *et al.* 2010) or followed by a main shock (e.g. Smith *et al.* 2008) are clearly driven by tectonic stresses (with, in some

*Now at: Department of Terrestrial Magnetism, Carnegie Institution of Washington, Washington, DC, USA. E-mail: droman@dtm.ciw.edu

†Now at: Department of Earth Sciences, University of Bristol, Bristol, UK.

cases, tectonic stresses exacerbated by circulation of geothermal fluids). However, numerous examples exist of earthquake swarms whose cause is not obvious even in hindsight. These swarms, which occur in regions of recent or active volcanism in the upper ~20 km of the crust, may be caused directly by intrusions of magma into the shallow crust. Alternatively, they may result from increased circulation of fluids above a deep intrusion of magma, perturbation of a geothermal system by a large regional earthquake, or some other process leading to intensification of tectonic stresses (e.g. 'strain transients' along subduction zones, McNutt & Marzocchi 2004).

Detailed investigation of these enigmatic earthquake swarms is critical for the development of a full understanding of the physical processes that drive earthquake swarms. An understanding of the process(es) which caused an earthquake swarm is, in turn, necessary for an accurate assessment of the potential hazards indicated by the swarm. Specifically, an accurate assessment of whether an earthquake swarm represents a failed eruption or a failed main shock is critical for understanding the level of volcanic and seismic hazard in the region. Careful documentation and analysis of earthquake swarms thus form a framework for understanding the range of processes that may drive earthquake swarms, and a context for interpretation during future episodes of geophysical unrest.

Here we investigate an intense earthquake swarm that occurred at Strandline Lake, Alaska, in 1996–1998. The cause of this swarm is unknown, but the location of the swarm volume at the northeastern edge of Aleutian arc indicates that it may be an intrusive or proto-volcanic extension of the arc, possibly related to the complex triple-junction tectonics centred on the area. Seismological analysis of the swarm earthquakes is limited by the sparse seismic network around Strandline Lake, and the limited availability of waveforms from key seismic stations located to the north and east of Strandline Lake. However, by combining waveform recordings from two permanent seismic networks operating in the area, we are able to analyse 50 of the largest swarm earthquakes to provide a characterization of the 1996–1998 swarm. We supplement this seismological analysis with an analysis of synthetic aperture radar (SAR) images of the Strandline Lake area. Although we are ultimately unable to determine the exact cause of the 1996–1998 Strandline Lake swarm, we document key details of the swarm and background earthquakes including locations, depths and source mechanisms, along with constraints on coseismic deformation. Based on this new information, we assess and constrain the possible causes of the swarm. Finally, our results are used to formulate guidelines for additional work necessary to understand the specific cause of the 1996–1998 Strandline Lake swarm, and for geophysical monitoring during future swarms at Strandline Lake and other earthquake swarms worldwide.

1.1 Strandline Lake, Alaska

Strandline Lake is located approximately 30 km northeast of Mt Spurr volcano and 110 km west of Anchorage, Alaska (Fig. 1). The lake is the result of damming of the Beluga River by the Triumvirate Glacier, and is subject to occasional outburst floods, or jökulhlaups, during melting or collapse of the glacier (Sturm & Benson 1985). The Strandline Lake region is underlain by Late-Cretaceous/Early Jurassic low-grade metamorphosed slate and volcanics, Palaeocene plutonic rocks composed mostly of granite, quartz monzonite and syenite, and older volcanic rocks (Wilson *et al.* 2009).

Strandline Lake is located in a complex tectonic setting at the northern end of the Aleutian volcanic arc, near the triple junction of the North American and Pacific plates and the subducting Yakutat

block, and between the Denali and Castle Mountain fault systems (fig. 2 of Eberhart-Phillips *et al.* 2006). Subduction of the Pacific plate beneath the North American plate has given rise to the Aleutian volcanic arc, one of the most active volcanic arcs in the world. Additionally, the Yakutat block, an exotic terrane, is actively accreting and subducting along the southern margin of Alaska (Brocher *et al.* 1994). Dextral transpression of the entire Cook Inlet area appears to be driven by coupling between the North American and Pacific plates, and by lateral escape of the Yakutat block (Haeussler *et al.* 2000). The three tectonic plates/blocks appear to converge somewhere near Strandline Lake. The Strandline Lake area is located directly within the Denali volcanic gap (e.g. Rondenay *et al.* 2010), an ~400-km-long segment of anomalously low volcanic activity extending from Mt Spurr to the 3000-yr-old Buzzard Creek Maars near Healy, Alaska. Strandline Lake is also directly aligned with the volcanic front formed by the active volcanoes in the Cook Inlet region (Mt Spurr/Crater Peak, Redoubt, Iliamna, Augustine and Fourpeaked, Fig. 1). The most recent eruption near Strandline Lake occurred at nearby Crater Peak (Mt Spurr) in 1992 (e.g. Eichelberger *et al.* 1995).

1.2 The 1996–1998 Strandline Lake earthquake swarm

In late 1996 August, an intense seismic swarm began beneath Strandline Lake (Fig. 2). The Alaska Volcano Observatory (AVO) earthquake catalogue (Jolly *et al.* 2001; Dixon & Stihler 2009) indicates that a total of 2507 earthquakes were recorded in the immediate vicinity of Strandline Lake between 1996 August 1 and 1998 September 30, in comparison to only 11 earthquakes from 1994 January 1 to 1995 December 31 and 184 earthquakes from 1999 January 1 to 2000 December 31. The higher post-swarm level of seismicity is most likely due to the presence of a local seismic station (STLK) installed in 1997. Seismic activity reached its peak rate on 1996 October 8, with 38 earthquakes recorded during one 24-h period (Figs 2a and d). All swarm earthquakes had waveforms similar to 'tectonic' earthquakes and indicative of brittle failure, with high-frequency codas and clear *P*- and *S*-wave arrivals (i.e. no long-period events or low-frequency tremor accompanied the swarm). The largest earthquake recorded during the Strandline Lake swarm was an M_L 3.6 on 1996 December 26, several months after the onset of the swarm (Figs 2b and e). Swarm and background earthquakes typically have catalogue magnitudes of less than M_L 2.0, and there does not appear to have been a significant change in earthquake magnitudes between the swarm and background periods (Fig. 2b). Using M_L magnitudes given in the AVO and Alaska Earthquake Information Center (AEIC) catalogues, we calculate a *b*-value of 1.01 (based on an M_L 0.5 magnitude of completeness) for the 1996–1998 swarm (Fig. 3a). We find a similar *b*-value of 1.12 (based on an M_L 0.5 magnitude of completeness) for background earthquakes at Strandline Lake (Fig. 3b), indicating that no significant increase in the *b*-value occurred between background and swarm periods. The cumulative seismic moment released during the swarm (assuming equivalence between M_L and M_W in continental Alaska, e.g. Ruppert & Hansen 2010) was approximately 1.2×10^{15} N m (Fig. 2e), equivalent to a single M_W 4.0 earthquake. While an earthquake with a magnitude of M_W 4.0 would not be expected to cause significant surface deformation, seismic swarms are frequently associated with magmatic intrusions, in which case the geodetically determined moment can be many times larger than the seismic moment, resulting in significant surface deformation (e.g. Biggs *et al.* 2009; Wright *et al.* 2006). Neither gas nor GPS monitoring was carried out at Strandline Lake during the

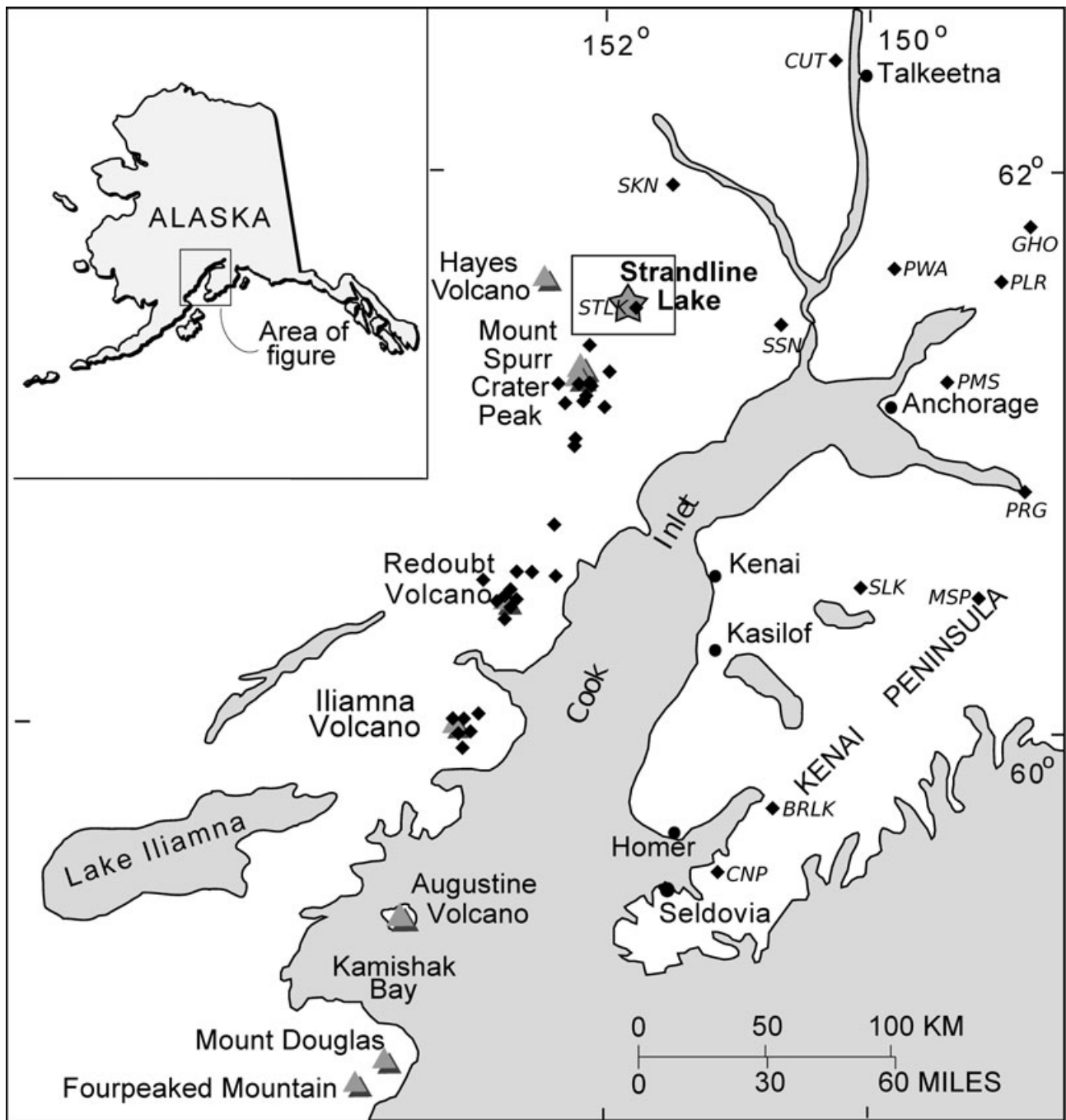


Figure 1. Map of the Cook Inlet region of Alaska showing the location of Strandline Lake (grey star) and its proximity to and alignment with the Cook Inlet volcanoes (grey triangles). Black diamonds represent seismic stations used for analysis in this study (names of stations are given in italics except for the Spurr, Redoubt and Iliamna networks), and black dots represent population centres. Black box indicates the bounds of the study area as described in the text.

swarm, and AVO did not receive any reports of anomalous activity (e.g. fumaroles, changes in lake water colour and increased glacial/snow melting) in the area during the period of seismic unrest.

2 SEISMIC OBSERVATIONS AND ANALYSIS

In this section, we present analyses of earthquakes recorded in the vicinity of Strandline Lake, Alaska. Our study area is de-

finied by a bounding box with coordinates $61^{\circ}24'N$, $61^{\circ}42'N$, $151^{\circ}30'W$ and $152^{\circ}15'$ (Fig. 1). We analyse earthquakes recorded between 1989 December 1 and 2009 September 30, and define the swarm period as 1996 August 1–1998 September 1. Seismological analysis is focused on 50 earthquakes occurring at Strandline Lake during swarm and background periods. These earthquakes were recorded clearly on seismic stations throughout the Cook Inlet region (Fig. 1), resulting in sufficient azimuthal coverage for the calculation of earthquake locations and fault-plane solutions.

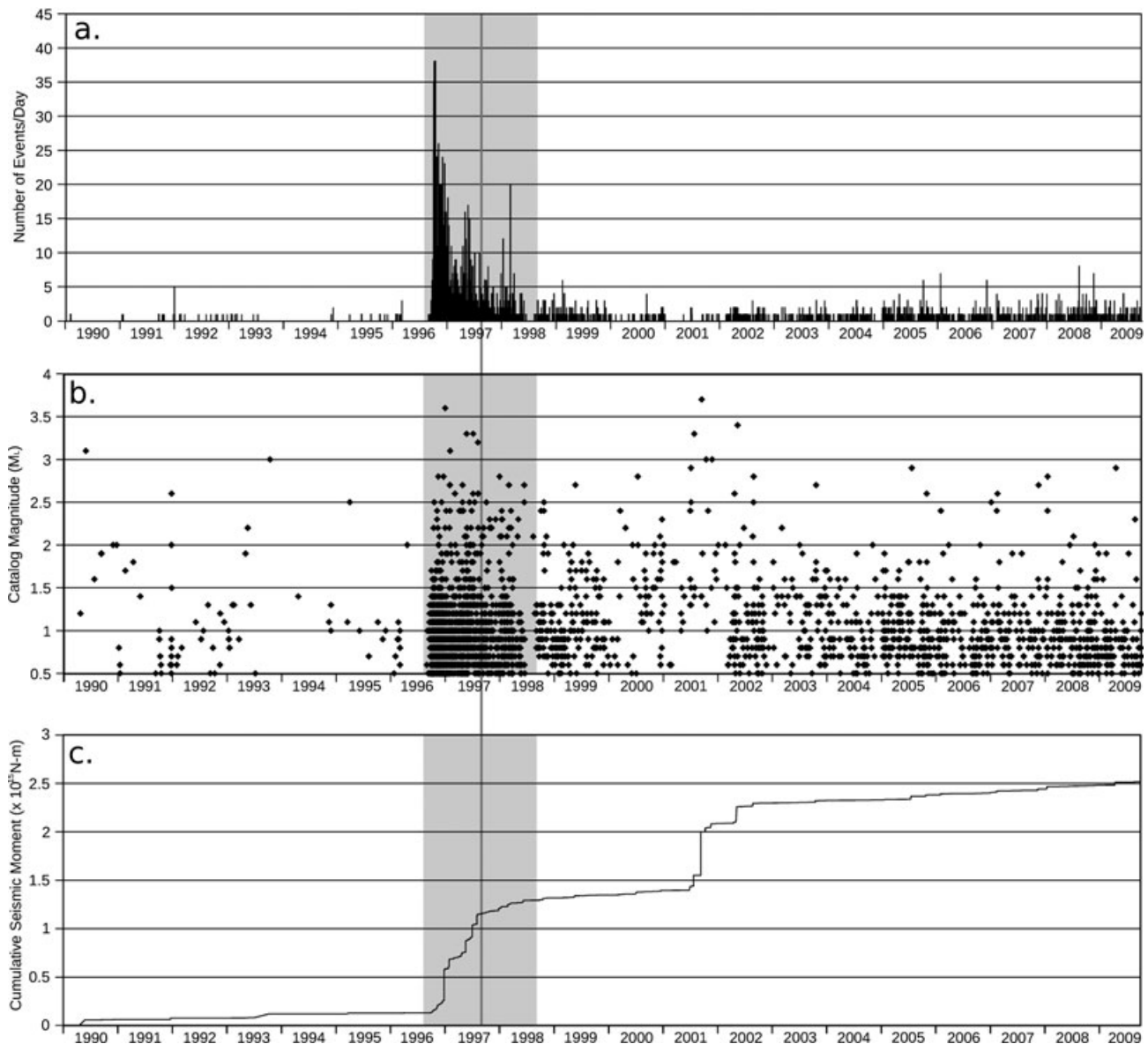


Figure 2. Rate, magnitude and cumulative seismic moment of earthquakes recorded at Strandline Lake between 1990 and 2009. Only earthquakes with magnitudes above the approximate magnitude of completeness ($0.5M_L$, see Fig. 3) are included in the plots. (a) Number of events recorded per day from 1990 to 2009. (b) Catalogue magnitudes (M_L) of earthquakes from 1990 to 2009. (c) Cumulative seismic moment (based on AVO catalogue magnitudes) from 1990 to 2009. (d) Number of events recorded per day during the swarm period (1996 August 1–1998 September 1). (e) Catalogue magnitudes (M_L) of earthquakes during the swarm period. (f) Cumulative seismic moment during the swarm period. The grey vertical lines indicate the date of installation of AVO seismic station STLK, and grey shaded areas in (a)–(c) indicate the time period plotted in Figs 2(d)–(f).

2.1 Geophysical monitoring

Seismic activity in the Strandline Lake area has been monitored continuously since the early 1990s by the AVO and AEIC. Seismic monitoring is the only method of continuous geophysical monitoring currently being conducted at Strandline Lake. The majority of the effective seismic network consists of seismometers installed and operated by AVO on Mt Spurr and Crater Peak, a vertical short-period seismic station (STLK) installed by AVO near Strandline Lake in 1997, midway during the swarm, and AEIC vertical short-period seismic stations SKN and SSN (Fig. 1). However, for larger Strandline Lake earthquakes, arrivals are also clearly recorded by the AVO seismic networks on Redoubt and Iliamna volcano, ~ 125 km and ~ 175 km to the south–southwest, respectively (Fig. 1), and on AEIC seismic stations to the east, northeast and

southeast of Strandline Lake (Fig. 1). Thus, for larger magnitude earthquakes, limited but adequate azimuthal coverage allows determination of earthquake locations and fault-plane solutions in the Strandline Lake area. Detailed specifications for all seismic stations used for analysis in this study are given in Table 1.

2.2 Velocity model and station corrections

Prior to this study, a 1-D velocity model developed for Mt Spurr (Jolly & Page 1994) was used by AVO to locate events at Strandline Lake. However, this model results in high average rms values and location errors, and may be inappropriate for the Strandline Lake area as it represents crust hosting a volcanic plumbing system. A second 1-D velocity model has been developed for southern Alaska

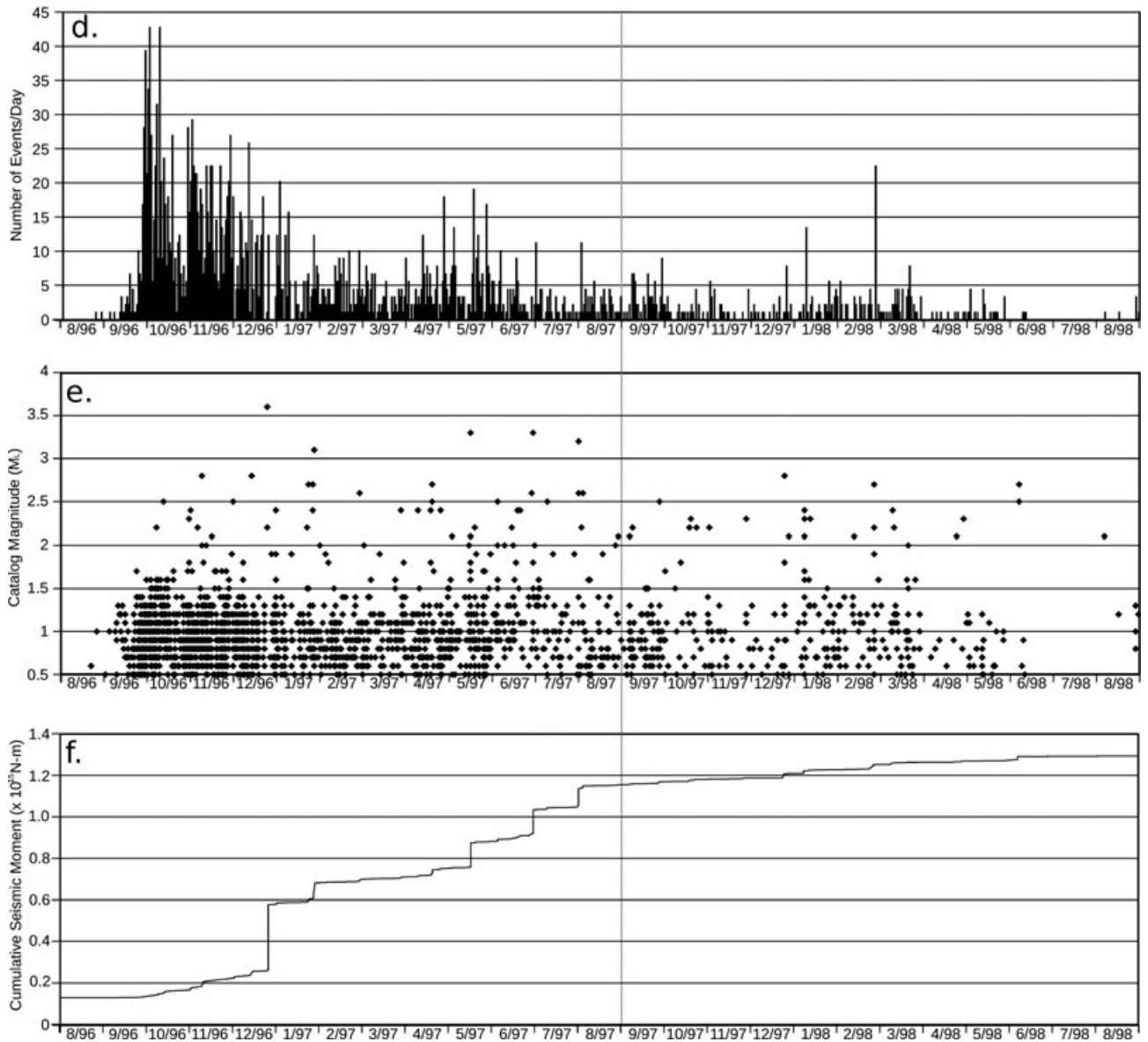


Figure 2. (Continued.)

(Fogleman *et al.* 1993) but also results in large average rms values and location errors for Strandline Lake earthquakes and thus may not be appropriate for our study area.

2.2.1 V_P/V_S ratio computation

To improve hypocentre depth estimates, an average V_P/V_S ratio was determined for the Strandline Lake area using a modified Wadati method (e.g. Chatelain 1978; Pontoise & Monfret 2004). A brief summary of the method is as follows: The differences in body wave arrival times P_i and P_j and S_i and S_j for an event k recorded by two stations (i, j) at hypocentral distances x_i and x_j are, respectively,

$$DT_P = P_i - P_j = (x_i - x_j)/V_P \quad (1)$$

and

$$DT_S = S_i - S_j = (x_i - x_j)/V_S. \quad (2)$$

Thus,

$$DT_S/DT_P = V_P/V_S, \quad (3)$$

and a plot of DT_S versus DT_P (Fig. 4) for 120 station-pair measurements indicates a V_P/V_S ratio of 1.73 for the Strandline Lake region. This value corresponds to a linear correlation coefficient of 0.99 and rms error of 0.51, and is similar to V_P/V_S values given by Eberhart-Phillips *et al.* (2006) of approximately 1.70–1.75 for the upper (<15 km below sea level, BSL) crust in the region between Mt Spurr and Denali.

2.2.2 1-D P -wave velocity model

To improve the accuracy of locations and fault-plane solutions for Strandline Lake earthquakes, we developed a new 1-D P -wave velocity model (Table 2) and associated station corrections (Table 3) for the Strandline Lake area using the joint inversion code VELEST (Kissling *et al.* 1994). VELEST inverts phase arrival time data for a set of input earthquakes using a joint hypocentre determination technique, and iterates to identify the 1-D model which results in locations with the lowest average rms for the input earthquakes.

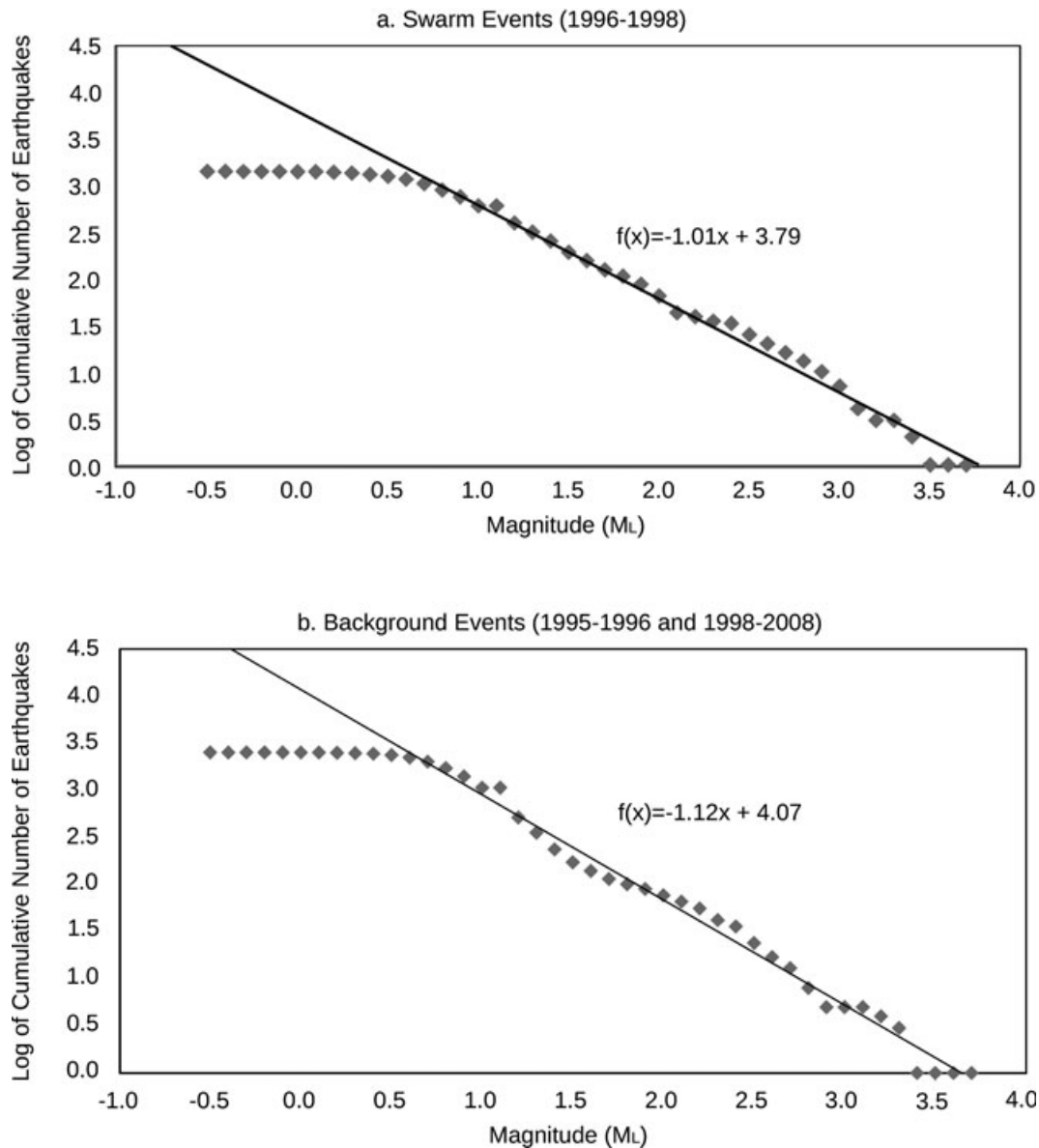


Figure 3. Frequency-magnitude distributions for (a) earthquakes occurring from 1996 September 1 to 1998 August 31 (the swarm period) and (b) background periods from 1995–1996 to 1998–2008. Black lines denote the best linear fit to the data above the magnitudes of completeness (M_L 0.5 for both periods). The slopes of these lines give the b -value for each period.

We sought a velocity model that minimized the average rms arrival time error for a set of 28 large Strandline Lake earthquakes by systematically perturbing the initial conditions for inversion of these events in VELEST. We repicked P -wave arrival times on the 39 stations listed in Table 1 for 28 large-magnitude (M_L 1.7–3.1) Strandline Lake earthquakes with clear and impulsive body wave arrivals to minimize rms due to picking error. To ensure that input earthquakes had an azimuthal gap $< 180^\circ$, we required a clear P -wave pick on stations SKN and SSN for all earthquakes, and a clear P -wave pick on local station STLK beginning in mid-1997. Furthermore, all 28 earthquakes had clear P -wave picks on the stations comprising the Spurr subnet (Table 1) as well as on a subset of the remaining 28 stations. S -wave picks were also included whenever the timing of the S -wave arrival could be identified precisely. The 1-D southern Alaska velocity model of Fogleman *et al.* (1993) was used as the starting model for the inversion. Starting with this ini-

tial velocity model and locations for the 28 input earthquakes, we ran VELEST to determine the best-fit locations and 1-D velocity model. If the resulting best-fit model had a large ($> 1 \text{ km s}^{-1}$) difference in V_p between adjacent model layers, we inserted an additional layer and repeated the inversion. If the resulting best-fit model had a small ($< 0.15 \text{ km s}^{-1}$) difference in V_p between adjacent layers, we deleted an additional layer and repeated the inversion. This process was repeated until a stable solution was obtained. As the Strandline Lake area is located in a mountainous region with significant topography, the top of the calculated 1-D velocity model extends to an elevation of 3 km above sea level (ASL).

The preferred velocity model, given in Table 2, has seven layers spanning a depth of 3 km ASL to 25 km BSL. Due to the paucity of three-component stations in the Strandline Lake area (limiting the availability of high-quality S -wave picks), VELEST was used to determine values for P -wave velocities only, and a constant V_p/V_s

Table 1. Description of seismic stations used for analysis in this study.

Station	Network	Subnet	Latitude	Longitude	Elev (m)	Sensor ^a
PDB	AVO		59° N47.27'	154° W11.55	305	L4
ILI	AVO	Iliamna	60° N04.88'	152° W57.50	771	L4
ILS	AVO	Iliamna	59° N57.45'	153° W04.08	1125	L4
ILW	AVO	Iliamna	60° N03.59'	153° W08.22	1646	L4
INE	AVO	Iliamna	60° N03.65'	153° W03.75	1585	L4
IVE	AVO	Iliamna	60° N01.01'	153° W00.98	1173	L22–3C
IVS	AVO	Iliamna	60° N00.55'	153° W04.85	2332	L4
DFR	AVO	Redoubt	60° N35.51'	152° W41.16	1090	L4
NCT	AVO	Redoubt	60° N33.73'	152° W55.76	1120	L4
RDN	AVO	Redoubt	60° N31.38'	152° W44.27	1400	L4
RDT	AVO	Redoubt	60° N34.39'	152° W24.32	930	L4
RDW	AVO	Redoubt	60° N28.96'	152° W48.57	1813	L4
RED	AVO	Redoubt	60° N25.19'	152° W46.31	1064	L4
REF	AVO	Redoubt	60° N29.36'	152° W41.50	1641	L22–3C
RSO	AVO	Redoubt	60° N27.73'	152° W45.23	1921	L4
BGR	AVO		60° N45.45'	152° W25.06	985	L4
BGL	AVO	Spurr	61° N16.01'	152° W23.34	1127	L4
BKG	AVO	Spurr	61° N04.21'	152° W15.76	1009	L4
CGL	AVO	Spurr	61° N18.46'	152° W00.40	1082	L4
CKL	AVO	Spurr	61° W11.78'	152° W20.27	1281	L4
CKN	AVO	Spurr	61° N13.44'	152° W10.89	735	L4
CKT	AVO	Spurr	61° N 12.05'	152° W12.37	975	L4
CP2	AVO	Spurr	61° N15.85'	152° W14.51	1981	L4
CRP	AVO	Spurr	61° N16.02'	152° W09.33	1622	L4–3C
NCG	AVO	Spurr	61° N24.22'	152° W09.40	1244	L4
SPU	AVO	Spurr	61° N10.90'	152° W03.26	800	L4
STLK	AVO		61° N29.93'	151° W49.96	945	L4
BRLK	AEIC		59° N45.83'	150° W53.38	622	L4
CNP	AEIC		59° N31.55'	151° W14.16	564	L4
CUT	AEIC		62° N24.28'	150° W16.17	168	L4
GHO	AEIC		61° N46.33'	148° W55.45	1021	L4
MSP	AEIC		60° N29.35'	149° W21.63	160	L4
PLR	AEIC		61° N35.53'	149° W07.85	100	L4
PMS	AEIC		61° N14.68'	149° W33.63	716	L4
PRG	AEIC		60° N51.87'	149° W01.21	55	L4
PWA	AEIC		61° N39.05'	149° W52.72	137	L4
SKN	AEIC		61° N58.82'	151° W31.78	564	L4–3C
SLK	AEIC		60° N30.74'	150° W13.26	655	L4
SSN	AEIC		61° N27.83'	150° W44.60	1297	L4

^aMark Products L-4 sensors have a natural frequency of 1 Hz, and Mark Products L-22 sensors have a natural frequency of 2 Hz. All sensors except CRP, REF, IVE and SKN are short-period, vertical instruments; CRP, REF, IVE and SKN are three-component short-period instruments. All AVO sensors are sampled at 100 Hz in both continuous and triggered modes; AEIC sensors are sampled at 120 Hz. For additional details on data acquisition and telemetry, please see, for example, Jolly *et al.* 2001 and Fogleman *et al.* 1993.

ratio of 1.73 is assumed based on the analysis presented in Section 2.2.1. Corresponding *S*-wave velocities for the preferred *P*-wave velocity model are given in Table 2. Seismic velocities in the upper crust at Strandline Lake increase with depth (Fig. 5) and range from 4.89 to 6.81 km s⁻¹ for *P*-waves and from 2.83 to 3.94 km s⁻¹ for *S*-waves. These velocities are slower than those in the Mt Spurr and Generic Alaska velocity models, but are similar to the velocities in a 1-D model obtained by Eberhart-Phillips *et al.* (2006) for southcentral Alaska. Compared the Generic Alaska velocity model, our new velocity model reduces the average rms of the 28 input earthquakes from 0.53 s to 0.14 s, and the average horizontal and vertical locations errors from 4.65 to 1.24 km and 6.90 to 2.29 km, respectively, indicating a significant improvement in location accuracy and quality. To further test the stability of this inversion, we performed a simple jackknife test by removing one station at a time from the inversion for the 28 stations contributing picks for some, but not all, of the 28 earthquakes. The resulting set of velocity mod-

els (shown as dashed lines in Fig. 5) shows an approximate range in *P*-wave velocity of 0.5 km s⁻¹ or less in all layers.

To further test the accuracy and stability of our new velocity model, we inverted a second set of 22 Strandline Lake earthquakes following the same procedure outlined earlier. These earthquakes were smaller in magnitude than the first set, but still had impulsive body wave arrivals that could be repicked with a high degree of accuracy. Again, we required clear *P*-wave picks on stations SKN and SSN for all earthquakes, and on local station STLK beginning in mid-1997. The resulting best-fit model reduced the average rms for the 22 input earthquakes from 0.42 s to 0.10 s, and the average horizontal and vertical locations errors from 4.41 to 1.38 km and 6.48 to 2.47 km, respectively, in comparison to those obtained using the Generic Alaska model. The second velocity model differs the preferred velocity model given in Table 2, with velocities again increasing with depth but ranging from 3.95 to 6.28 km s⁻¹ for *P* waves (Fig. 5), and from 2.28 to 3.63 km s⁻¹ for *S* waves.

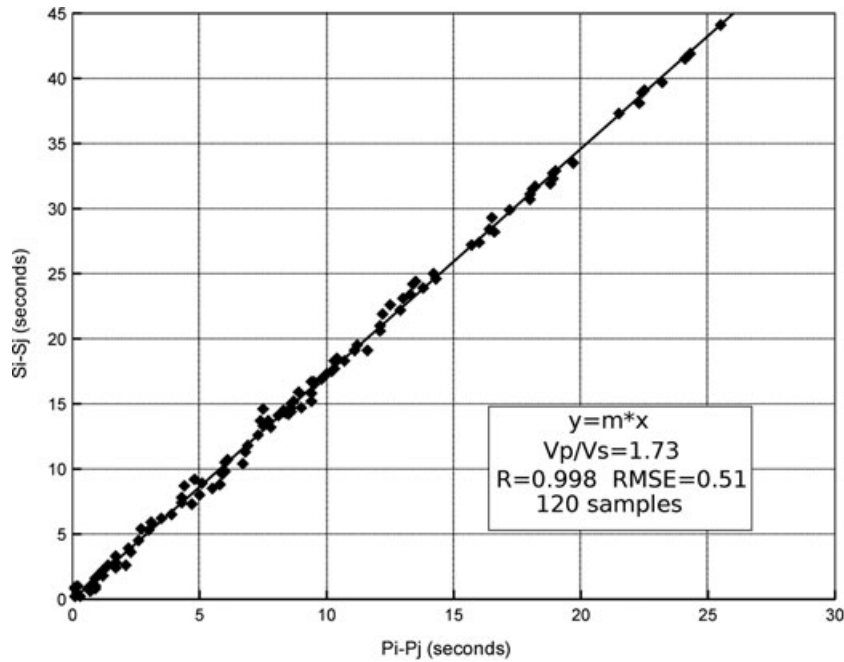


Figure 4. DT_S versus DT_P for Strandline Lake earthquakes. Linear fit gives the V_P/V_S ratio for the area (see text for details).

Table 2. New 1-D velocity model for the Strandline Lake area.

Depth to top of layer (km)	V_P (km s ⁻¹)	V_S (km s ⁻¹)
-3	4.89	2.83
-1	5.21	3.01
2	5.7	3.29
4	6.04	3.49
9	6.47	3.74
15	6.63	3.83
25	6.81	3.94

2.3 Earthquake locations

Best-fit earthquake locations from the VELEST joint inversions are plotted in map view and cross-section in Fig. 6. For comparison, we show all 50 earthquakes located with the preferred velocity model in Figs 6(a) and (b), and with the second velocity model in Figs 6(c) and (d). In both cases the epicentres form a small (~ 5 km radius), roughly circular cluster centred on the ‘peninsula’ of land between Strandline Lake and the Triumvirate glacier (Figs 6a and c). However, while the epicentral differences in locations obtained using preferred and second velocity models are minor (Figs 6a and c), hypocentre depths calculated using the second velocity model are considerably greater (~ 17 – 30 km BSL) and more scattered than those obtained with the preferred velocity model (~ 12 – 17 km BSL, Figs 6b and d). Therefore, while both models indicate that the swarm earthquakes are located below ~ 10 km BSL, the precise depths are not well constrained (and because STLK is a one-component seismometer, we cannot examine S – P arrival times to assess earthquake depth). While the absence of a local seismic station prior to 1997 is no doubt a major contributing factor, we note that the depths of earthquakes located before and after 1997 (i.e. with and without arrival time picks from local station STLK) are similar. Because we have higher confidence in the pick accuracy for the first set of earthquakes, we use the velocity model obtained with the 28 larger earthquakes, and given in Table 2 for the remainder of our analysis. However, given the depth differences apparent in

Table 3. Station corrections for the 1-D Strandline Lake velocity model presented in Table 2.

Station name	Correction (s)	Station name	Correction (s)
BGL	-0.41	IVS	-0.02
BGR	-0.38	MSP	0.47
BKG	-0.42	NCG	-0.67
BRLK	-0.05	NCT	-0.01
CGL	-0.81	PDB	0.11
CKL	-0.59	PLR	0.72
CKN	-0.21	PMS	0.66
CKT	-0.47	PRG	0.63
CNP	-0.45	PWA	1.05
CP2	-0.77	RDN	-0.15
CRP	-0.65	RDT	-0.33
CUT	1.71	RDW	-0.09
DFR	-0.19	RED	-0.32
GHO	0.77	REF	-0.14
ILI	-0.15	RSO	-0.11
ILS	0.06	SKN	1.37
ILW	0.04	SLK	0.24
INE	-0.09	SPU	-0.54
IVE	-0.01	SSN	0.25

Fig. 6, we note that the formal errors for subsequent analyses are likely underestimated as they do not take into account any errors in the velocity model.

2.4 Composite fault-plane solutions

Analysis of double-couple fault-plane solutions for swarm and background earthquakes may be useful in constraining the cause of an earthquake swarm. However, due to the paucity of seismic stations to the northwest, southeast and immediate vicinity of Strandline Lake (Fig. 1), it is difficult to produce well-constrained fault-plane solutions for Strandline Lake earthquakes. In such cases, it may still be possible to determine some of the characteristics of both swarm and background earthquake focal mechanisms through the construction

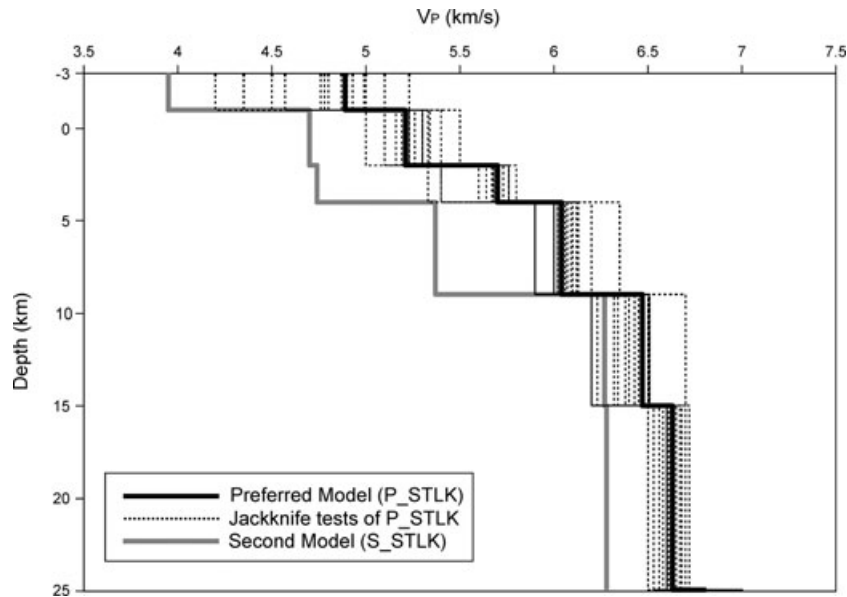


Figure 5. *P*-wave velocity models obtained with VELEST. Heavy black line shows the preferred velocity model obtained from inversion of 28 large-magnitude earthquakes, and fine dashed lines show the results of a jackknife test of the stability of the preferred velocity model (see text for details). Heavy grey line shows a second velocity model obtained from inversion of 22 additional Strandline Lake earthquakes.

of composite fault-plane solutions. Using FPFIT (Reasenber & Oppenheimer 1985) we produced two composite double-couple fault-plane solutions, one for background earthquakes and another for swarm earthquakes. Both composite solutions are based only on earthquakes with well-constrained locations (six or more *P*-wave arrival picks, azimuthal gap $<180^\circ$, rms <0.20 s, and vertical and horizontal location error <3 km) and six or more clear first-motion polarities. Following these criteria, we identified six background earthquakes with a total of 60 clear first-motion polarity picks to constrain a background composite fault-plane solution, and 20 swarm earthquakes with a total of 263 clear first-motion polarity picks to constrain a swarm composite focal mechanism. The resulting best-fit fault-plane solutions are shown graphically, along with 95 per cent confidence regions for *P*- and *T*-axis positions, in Fig. 7, and their parameters are listed in Table 4.

The best-fit composite solutions for background and swarm periods differ significantly in their orientations (Fig. 7). Only one possible fault-plane solution was obtained for the six background earthquakes (Fig. 7a). This solution indicates oblique thrust motion on an east–west or northeast–southwest trending fault with a significant component of strike-slip motion. The *P*-axis is oriented NW and is almost horizontal, and the *T*-axis is oriented WSW, with a dip of 49° (Table 4). There are three possible solutions for the swarm earthquake polarities (Figs 7b and d). One of the three possible swarm solutions shows oblique slip on a near-vertical or near-horizontal fault, with a small component of strike-slip motion. The other two solutions show oblique thrust faulting on an east–west or northwest–southeast trending fault with a small component of strike-slip motion. The *P*- and *T*-axis azimuths are similar (NNE to NE; NW to WNW) in all three possible solutions. However, the *P*- and *T*-axis dips are more variable and thus less well constrained. The apparent difference in the orientation of the best-fit composite solutions suggests that the swarm earthquakes were driven by a different mechanism than background earthquakes at Strandline Lake.

The percentage of misfit first-motion polarities in the best-fit composite solution also differs between the swarm and background

earthquakes; The misfit between the polarity data and the best-fit solution is much lower for the swarm composite solution (9 per cent, or 23 first-motion polarities out of 263) than for background composite solution (20 per cent, or 12 polarities out of 60). Potential sources of misfit polarities in a composite fault-plane solution include picking errors [e.g. picking an up first-motion rather than a (correct) down first-motion], failure to correct for stations with reversed polarities (stations that record true up first-motions as down first-motions on the seismogram), errors in the earthquake location and/or velocity model resulting in incorrect placement of a first-motion polarity on the focal sphere, and heterogeneity in the orientations of the fault-plane solutions for the earthquakes used to create the composite solution. While it is possible that some component of picking error and reversed-station-polarity error may account for the misfit polarities (we only picked clear first-motions and corrected for all known stations with reversed polarities), it is most likely that the misfit polarities are due to a combination of location/velocity model error (background fault-plane solution (FPS) earthquake locations are more dispersed than those for swarm earthquakes) and true heterogeneity in individual earthquake fault-plane solutions.

3 InSAR ANALYSIS AND OBSERVATIONS

A continuous GPS (cGPS) monitoring network did not exist in the remote regions surrounding the Cook Inlet in Alaska in 1996–1998. To supplement the seismic data analysis presented in Section 2, we produced interferograms using images acquired by the SAR instrument on board the ERS-2 satellite. Image pairs from before, during and after the swarm period were analysed to detect any temporal changes in ground elevation that may have accompanied the swarm.

The ERS-2 satellite was launched in 1995 April and frequently made passes over the southern Alaska region. A search of ERS-2's archives yielded 49 images along descending track 229 which captured the Strandline Lake area. Of the 49 images, 18 were selected based upon time-of-capture (1995–1999) relative to the swarm. Four

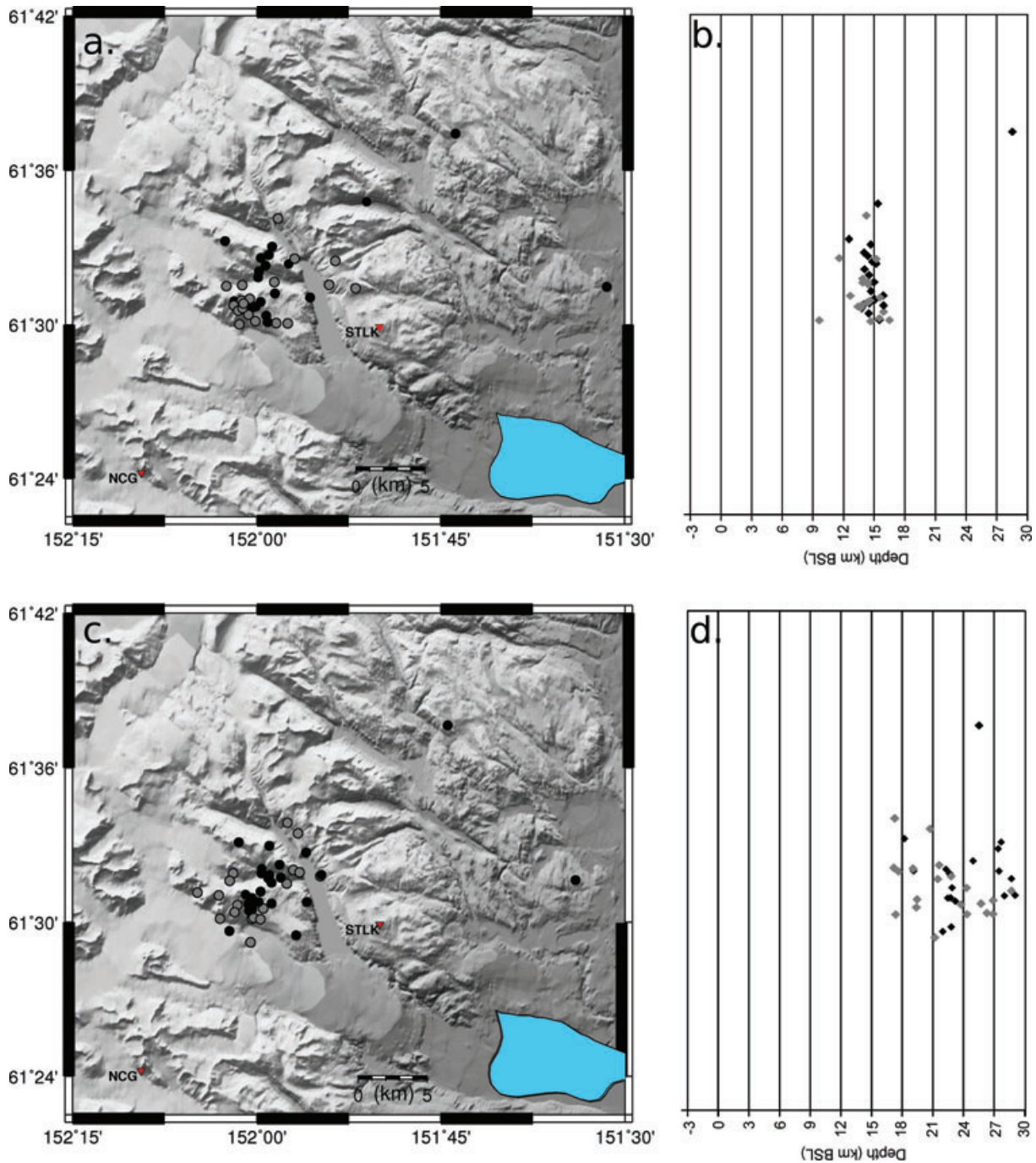


Figure 6. Map and N–S cross-sections showing the locations of 50 large-magnitude earthquakes relocated with (a,b) the preferred velocity model resulting from inversion of 28 earthquakes and (c,d) a second velocity model resulting from inversion of 22 additional earthquakes. Black symbols indicate earthquakes used to determine the preferred model; grey symbols indicate earthquakes used to determine the second model.

of the selected images were taken prior to the swarm (1995–1996), six during the swarm (1996–1998) and the remaining eight were taken post-swarm (1998–1999). Interferograms were then processed using the Repeat Orbit Imagery Package (*roi_pac*) software (CalTech/JPL). For successful interferogram processing, the two images to be compared needed to have a small perpendicular baseline and to cover a short time span. Limits of 250 m and 3 yr were chosen as the boundaries of these parameters and a total of 56 interferograms (event pairs) met these conditions. Of these 56 event pairs, only those with highly coherent signals were used in further analysis.

This reduced the final number of event pairs to 18. Topographic effects in the interferograms were removed during the interface with a National Elevation Dataset (NED) 2-arc-second Digital Elevation Map (DEM) obtained from the U.S. Geological Survey National Map Seamless Server. Each colour cycle (fringe) on the interferogram represents 2.8 cm of deformation, and error associated with atmospheric properties is typically <1 cm.

A total of 13 InSAR image pairs (Table 5) were found to have coherence in the Strandline Lake area. The 13 image pairs were examined individually for any indication of surface deformation

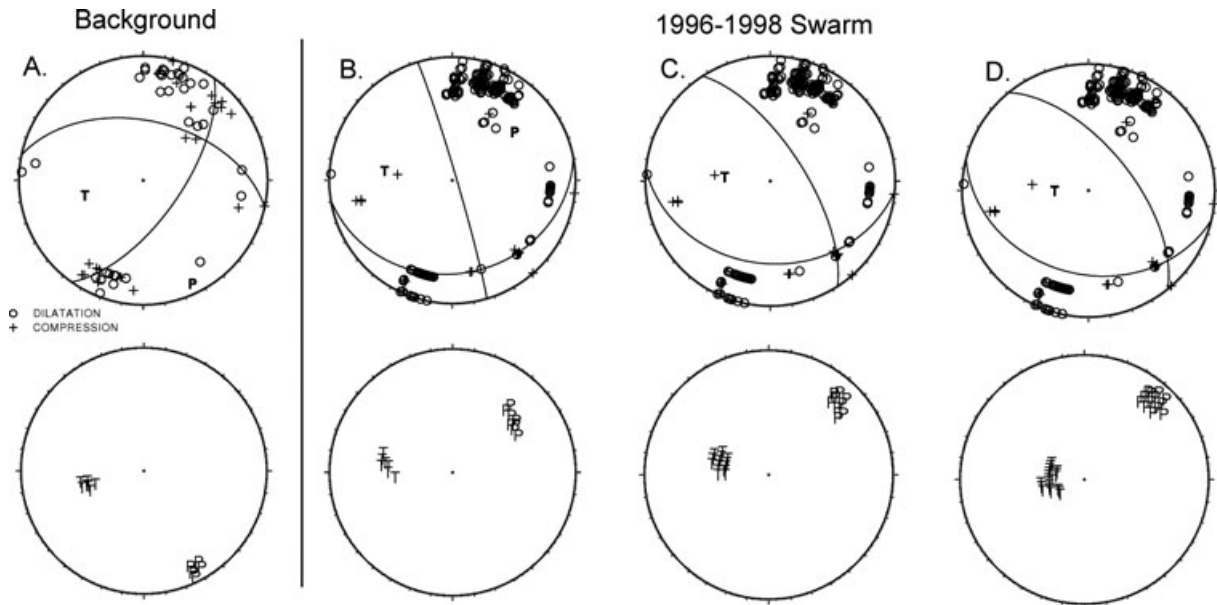


Figure 7. Composite fault-plane solutions for (a) six background earthquakes and (b–d) 20 swarm earthquakes (three possible solutions). The top row shows the graphical fault-plane solution, including first-motion polarity data (circles and plus signs), and the bottom row shows the 95 per cent confidence regions for the pressure (P) and tension (T) axes. Additional information, including the percentage of misfit first-motion data for each solution, is given in Table 4.

associated with the Strandline Lake swarm. Particular attention is given to image pairs which have dates pre- and during swarm and during and post-swarm. One such InSAR image is shown in Fig. 8. Only five of the 13 images yielded high-quality results while the rest exhibited abundant background noise which appears pixelated and provides little insight into surface deformation. Factors such as the considerable topographic relief of the adjacent Tordrillo Mountains, the abundant snow cover in the area and the presence of a moving glacier possibly attributed to the low quality of the other eight InSAR images. Fringes in the high-quality InSAR images of the Strandline Lake area have long distances between them and appear broad. Slight (<2 cm) changes in surface elevation may have occurred, however, any deformation exhibited in the InSAR images of Strandline Lake likely falls outside the margin of error associated with the instruments onboard the ERS-2 satellite. The Triumvirate glacier is adjacent to Strandline Lake and any changes in elevation found within its area can be attributed to the mechanics of the glacier. While each InSAR image of Strandline Lake has its own unique characteristics, none show the typical ‘bullseye’ patterns indicative of inflation of a spherical chamber or double lobes indicative of dyke intrusion (e.g. Lu *et al.* 2000, 2007).

4 DISCUSSION

Several possible causes of the 1996–1998 Strandline Lake swarm may be ruled out on the basis of existing evidence. There was no obvious main shock located in the immediate vicinity of the swarm volume. However, to rule out the possibility that the Strandline Lake swarm may have been an aftershock sequence related to a non-local main shock, we searched the AEIC catalogue for shallow (<50 km deep) earthquakes with $M > 4.0$ located in the vicinity of Strandline Lake. Three earthquakes met these criteria, but preceded the onset of the Strandline Lake swarm by 4–6 months. Although it is possible that the swarm represents a set of spatially and temporally delayed aftershocks to one or more of these events, it is not highly plausible. The Castle Mountain Fault experienced a shallow (~ 17 km BSL) $M4.6$ earthquake only 120 km from Strandline Lake

in November of 1996 (Haeussler 2000); however, as this event occurred after the swarm onset, it can also be ruled out as a cause of the swarm. Another possible cause which may be ruled out is sudden unloading due to a jökulhlaup at the glacially dammed Strandline Lake: First, there were no recorded jökulhlaups at Strandline Lake between 1991 August and 1999 August (Ben Balk, NOAA, personal communication, 2004). Secondly, the swarm depth and cumulative seismic moment appear to be inconsistent with the low degree of surface unloading that would be associated with a small jökulhlaup typical of Strandline Lake (Sturm & Benson 1985). A third possible cause which may be ruled out is a slow-slip earthquake, which are known to occur in the eastern Aleutians and which could hypothetically trigger a swarm-like aftershock sequence. No slow-slip earthquakes were detected in the eastern Aleutians in 1996, prior to the swarm onset, although a major slow-slip earthquake detected in 1998 was located immediately downdip of the rupture plane for the great 1964 Alaska earthquake and approximately 100 km due east of the Strandline Lake swarm volume (Ohta *et al.* 2006).

Two probable causes of the 1996–1998 Strandline Lake swarm remain after consideration of all available observations. The first probable cause of the swarm is a reduction in effective normal stresses in the swarm volume due to an episode of deep (non-magmatic) fluid circulation (e.g. Scholz 2002). Although many earthquake swarms worldwide are believed to be driven by fluid circulation, the nature of the hypothesized episodes of fluid circulation is often poorly understood, and triggering mechanisms for bursts of increased fluid circulation during earthquake swarms are generally unconstrained. One possible trigger for an episode of fluid circulation is a ‘hidden’ stalled magma intrusion, either within the crust or at the base of the overriding plate (e.g. Rondenay *et al.* 2010). Alternatively, pulses of increased fluid circulation may simply be manifestations of a more steady-state phenomenon such as dewatering of a subducting slab. The second probable cause of the Strandline Lake swarm is direct triggering through an increase in shear stress in the swarm volume imposed by deep magma intrusion. Non-eruptive swarms known to be caused by magma intrusion are often accompanied by other indicators of volcanic unrest such as increased gas emissions

Table 4. Composite fault-plane solutions and input earthquakes for (a) swarm and (b) background periods at Strandline Lake.

Date	Time	Latitude	Longitude	Depth (km BSL)	Magnitude (M_L)	No. of polarities	Strike 1	Dip 1	Rake 1	Strike 2	Dip 2	Rake 2	P-axis azimuth	P-axis dip	T-axis azimuth	T-axis dip	Misfit
(a)	Composite	—	—	—	—	263	80	25	7	344	87	115	52	37	277	43	0.09
	Composite	—	—	—	—	263	95	34	43	327	68	116	38	18	275	59	0.09
	Composite	—	—	—	—	263	104	34	58	321	62	110	37	15	269	67	0.1
11/02/96	05:38:02	61N32.72	151W59.02	14.07	2.4	12	—	—	—	—	—	—	—	—	—	—	—
11/10/96	16:52:04	61N31.22	151W58.51	14.74	2.2	16	—	—	—	—	—	—	—	—	—	—	—
12/02/96	11:20:48	61N30.35	151W59.23	14.52	2.0	15	—	—	—	—	—	—	—	—	—	—	—
01/23/97	20:49:53	61N32.29	151W59.28	15.26	2.2	16	—	—	—	—	—	—	—	—	—	—	—
01/24/97	21:28:00	61N32.07	151W59.81	14.11	2.5	16	—	—	—	—	—	—	—	—	—	—	—
01/27/97	03:46:16	61N32.43	151W58.42	13.57	1.6	7	—	—	—	—	—	—	—	—	—	—	—
01/27/97	04:36:33	61N32.59	151W59.66	14.44	2.5	13	—	—	—	—	—	—	—	—	—	—	—
01/28/97	20:45:25	61N32.34	151W58.25	14.79	2.9	17	—	—	—	—	—	—	—	—	—	—	—
02/11/97	16:22:07	61N31.85	151W59.89	14.55	1.4	10	—	—	—	—	—	—	—	—	—	—	—
05/05/97	11:39:44	61N30.76	152W01.86	14.54	1.5	11	—	—	—	—	—	—	—	—	—	—	—
05/18/97	22:11:20	61N30.70	152W00.08	14.05	2.0	14	—	—	—	—	—	—	—	—	—	—	—
05/21/97	16:31:26	61N30.15	152W00.11	15.71	2.0	17	—	—	—	—	—	—	—	—	—	—	—
05/22/07	13:27:43	61N30.10	151W59.10	15.57	2.0	10	—	—	—	—	—	—	—	—	—	—	—
06/01/97	12:41:58	61N30.78	152W01.76	14.27	1.8	12	—	—	—	—	—	—	—	—	—	—	—
06/06/97	20:00:42	61N31.51	152W02.46	14.29	1.9	16	—	—	—	—	—	—	—	—	—	—	—
06/11/97	11:54:42	61N30.80	152W02.14	14.44	1.7	10	—	—	—	—	—	—	—	—	—	—	—
06/20/97	02:08:48	61N31.38	152W01.31	14.32	1.8	10	—	—	—	—	—	—	—	—	—	—	—
06/22/97	18:08:37	61N30.65	152W01.14	13.94	1.7	12	—	—	—	—	—	—	—	—	—	—	—
09/09/97	16:06:37	61N30.55	152W01.51	13.83	1.8	17	—	—	—	—	—	—	—	—	—	—	—
02/12/98	00:34:48	61N30.46	151W59.73	14.47	1.6	12	—	—	—	—	—	—	—	—	—	—	—
(b)	Composite	—	—	—	—	60	35	65	45	282	50	147	155	9	256	49	0.2
05/26/90	08:16:37	61N33.26	151W55.40	13.3	3.1	8	—	—	—	—	—	—	—	—	—	—	—
09/05/90	17:55:40	61N36.95	152W01.58	13.22	1.9	12	—	—	—	—	—	—	—	—	—	—	—
12/20/91	14:57:01	61N30.95	151W55.09	16.37	2.0	10	—	—	—	—	—	—	—	—	—	—	—
05/14/93	19:36:00	61N37.32	152W02.30	12.3	2.2	9	—	—	—	—	—	—	—	—	—	—	—
11/06/94	08:53:48	61N23.71	151W53.97	24.84	1.6	8	—	—	—	—	—	—	—	—	—	—	—
04/16/96	05:04:30	61N32.52	151W37.54	14.21	2.0	13	—	—	—	—	—	—	—	—	—	—	—

Table 5. Dates of image pairs for the 13 InSAR images produced for this study. Image pairs in bold indicate high-quality InSAR images. Asterisks indicate images used for example interferogram presented in Fig. 8.

Date 1	Date 2
06/19/96*	07/09/97*
07/24/96	07/14/99
10/02/96	06/04/97
10/02/96	07/09/97
06/04/97	07/29/98
07/09/97	08/13/97
07/09/97	07/29/98
07/09/97	09/02/98
07/29/98	09/02/98
09/02/98	06/09/99
09/02/98	09/22/99
10/07/98	07/14/99
06/09/99	07/14/99

(e.g. Roman *et al.* 2004) or surface deformation (e.g. Toda *et al.* 2002; Smith *et al.* 2004). At Strandline Lake, it is unknown whether any coincident indicators of magma intrusion were present during the 1996–1998 swarm. Gas monitoring was not conducted, and although we did not detect surface deformation during the swarm through InSAR analysis, subcentimetre-scale surface uplift cannot be ruled out based on our deformation analysis. Thus, on the basis of available evidence, we may conclude that the 1996–1998 Strandline Lake earthquake swarm was driven either by fluid circulation or directly by magma intrusion, but the existing observations do not allow us to favour either one of these mechanisms. Given that other recent deep earthquake swarms driven by lower crustal magma intrusion have been accompanied by subcentimetre-scale surface uplift (e.g. Smith *et al.* 2004) it will be critical to implement cGPS monitoring at Strandline Lake during any future earthquake swarms.

A promising approach to determining the proximal cause of a non-volcanic earthquake swarm (i.e. fluid circulation or magma intrusion) is analysis of the local crustal stress field in the region

hosting the swarm. The results of several recent studies of local stress field orientation preceding volcanic eruptions have shown that a systematic change in the orientation of local principal stress axes occurs in the weeks to months prior to an eruption, reflecting an ephemeral local stress field produced by the ascent of magma through the shallow crust (e.g. Gerst & Savage 2004; Roman & Cashman 2006). Specifically, a local axis of maximum compression oriented $\sim 90^\circ$ to regional maximum (horizontal) compression is observed during periods of inflation of a dyke-like volcanic conduit. Thus, earthquake swarms that are directly driven by magma intrusion may be characterized by both an increase in the local rate of seismicity and a systematic $\sim 90^\circ$ change in the local stress field orientation, while earthquake swarms driven by fluid circulation may be characterized by an increase in seismicity rate but no $\sim 90^\circ$ change in local stress field orientation (though smaller degrees of stress field reorientation may occur due to slip on non-ideally oriented faults in response to increased pore pressures.) Therefore, careful comparison of the local stress field orientation during an earthquake swarm to the local stress field orientation during periods of background levels of seismicity should give a clear indication of the proximal cause of the swarm. At Strandline Lake, the local stress field during the 1996–1998 swarm is characterized by a composite FPS with a NE P -axis orientation (Figs 7b and d). However, the orientation of the background stress field at Strandline Lake is unclear (Fig. 7a), making it difficult to assess whether the NE P -axis trend observed during the swarm is rotated with respect to the background orientation or not. A study of split S -wavelet polarizations for regional earthquakes recorded on the AEIC three-component station SKN, located to the NE of Strandline Lake (Fig. 1) indicates a background stress field characterized by a NE-oriented regional maximum compression (σ_1) axis (Wiemer *et al.* 1999). However, FPS for regional and background earthquakes located at or near the volcanoes of the Cook Inlet indicate a NW-oriented σ_1 axis to the southwest of Strandline Lake (e.g. Jolly *et al.* 1994; Sanchez *et al.* 2004; Roman *et al.* 2004; Ruppert 2008), and focal mechanisms for regional earthquakes located in a large region extending southwards from the Denali Fault through the upper Cook Inlet region indicate an E–W oriented σ_1 axis (Ruppert 2008). Thus, Strandline Lake appears to be located in a transitional tectonic zone between the eastern Aleutians, characterized by a spatially variable crustal stress field (e.g. Plates 4 and 5 of Ruppert 2008) and bounded by a

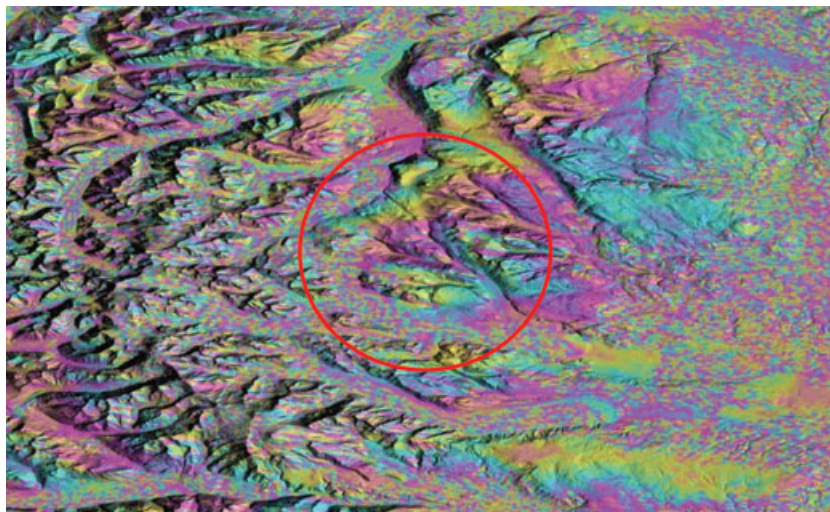


Figure 8. Example InSAR image of Strandline Lake, Alaska, showing lack of evidence for surface deformation during the swarm. The SAR images used for this figure were captured on 1996 June 19 (pre-swarm) and 1997 July 9 (mid-swarm). The red circle indicates the approximate location of swarm epicentres.

region of NW-oriented maximum compression due to convergence of the North American and Pacific plates, and a region characterized by NE-oriented maximum compression driven by southwestward escape of the subducting and accreting Yakutat terrane. Thus, installation of a temporary or permanent network of three-component seismometers in the vicinity of Strandline Lake is necessary for a detailed characterization of the ‘background’ tectonic stress field in the immediate vicinity of the swarm through analysis of split *S*-wavelet polarizations, and subsequent interpretation of the local stress field orientation observed during the 1996–1998 swarm.

5 CONCLUSIONS

We have documented and analysed a major earthquake swarm recorded at Strandline Lake, Alaska, in 1996–1998, which consisted of approximately 2500 earthquakes recorded over a period of 22 months. We relocated 50 of the largest magnitude events using a newly developed 1-D velocity model. All events were located at depths of greater than ~10 km BSL, and swarm epicentres form a small, roughly circular cluster. Background seismicity at Strandline Lake occurs at a low rate and earthquake epicentres are more widely dispersed than swarm events, but background earthquakes locate in approximately the same depth range as swarm events. Three best-fit composite fault-plane solutions for 20 swarm earthquakes have a low misfit to first-motion polarity data, and indicate a NE-oriented *P*-axis. In contrast, a composite fault-plane solution for six background earthquakes has a high misfit to the first-motion polarity data, making it difficult to determine the ambient stress field orientation at Strandline Lake. No deformation was detected during the swarm by InSAR analysis, though we are unable to rule out the possibility of subcentimetre deformation due to the lack of cGPS monitoring during the swarm. We conclude that the 1996–1998 earthquake swarm was likely caused either by an episode of deep magma intrusion or by deep fluid circulation (which in turn may have been a consequence of deeper magma intrusion). In either case, the Strandline Lake area may represent a ‘cryptovolcanic’ extension of the Aleutian arc towards Denali, where subduction of the Yakutat terrane may be driving weak lower and mid-crustal magmatism that does not culminate in surficial volcanic activity (e.g. Nye *et al.* 2002; Rondenay *et al.* 2010).

ACKNOWLEDGMENTS

This study was funded by NSF EAR0809823 to DR and JP. ERS data are from the European Space Agency through GeoEarthScope. JB was supported by a Rosenstiel Fellowship at the University of Miami. We gratefully acknowledge John Power for his assistance with this study and manuscript. We thank Matthew Sturm and Ben Balk for unpublished information about jokulhlaups at Strandline Lake. We also thank Natalia Ruppert, Mitch Robinson and Tom Parker for assistance with data retrieval, and Chris Nye for an interesting discussion on possible lower crustal magmatism in the Strandline Lake–Denali region. Finally, we gratefully acknowledge Diane Doser and Josef Horalek for their insightful and constructive reviews of this manuscript.

REFERENCES

- Ake, J., Mahrer, K., O’Connell, D. & Block, L., 2005. Deep-injection and closely monitored induced seismicity at Paradox Valley, Colorado, *Bull. seism. Soc. Am.*, **95**, 664–683.
- Benoit, J.P. & McNutt, S.R., 1996. Global volcanic earthquake swarm database 1979–1989. *U.S. Geol. Surv. Open-File Rep.*, **96–69**, 31pp.
- Biggs, J., Amelung, F., Gourmelen, N. & Dixon, T., 2009. InSAR observations of 2007 Tanzania seismic swarm reveals mixed fault and dyke extension in an immature continental rift, *Geophys. J. Int.*, **179**, 549–558.
- Brocher, T.M., Fuis, G.S., Fischer, M.A., Plafker, G., Moses, M.J., Taber, J.J. & Christensen, N.I., 1994. Mapping the megathrust beneath the northern Gulf of Alaska using wide-angle seismic data, *J. geophys. Res.*, **99**, 11 663–11 685.
- Chatelain, J.L., 1978. Etude fine de la sismicite en zone de collision continentale a l’aide d’un reseau de statios portables: la region Hindu-Kush-Pamir. *PhD thesis*, Univ. Paul Sabatier, Toulouse.
- Dixon, J.P. & Stihler, S.D., 2009. Catalog of earthquake hypocenters at Alaskan volcanoes: January 1 through December 31, 2008. *U.S. Geol. Surv. Data Series*, **467**, 88pp.
- Dorbath, L., Evans, K., Cuenot, N., Valley, B., Charlety, J. & Frogneux, M., 2010. The stress field at Soultz-sous-Forêts from focal mechanisms of induced seismic events: cases of the wells GPK2 and GPK3, *Comptes Rendus. Geosci.*, **342**, 600–606.
- Eberhart-Phillips, D., Christensen, D.H., Brocher, T.M., Hansen, R.A., Ruppert, N.A., Haeussler, P.J. & Abers, G.A., 2006. Imaging the transition from Aleutian subduction to Yakutat collision in central Alaska, with local earthquakes and active source data, *J. geophys. Res.*, **111**, B11303, doi:10.1029/2005JB004240.
- Eichelberger, J.C., Keith, T.E.C., Miller, T.P. & Nye, C.J., 1995. The 1992 eruptions of Crater Peak Vent, Mount Spurr Volcano, Alaska: chronology and summary, in *The 1992 Eruptions of Crater Peak Vent, Mount Spurr Volcano, Alaska*, U.S. Geological Survey Bulletin B-2139, pp. 1–18, ed. Keith, T.E.C., USGS, Reston, VA.
- Fogleman, K.A., Lahr, J.C., Stephens, C.D. & Page, R.A., 1993. Earthquake locations determined by the Southern Alaska Seismograph Network for October 1971 through May 1989, *U.S. Geol. Surv. Open-File Rep.*, **93–309**, 54pp.
- Gerst, A. & Savage, M.K., 2004. Seismic anisotropy beneath Ruapehu Volcano: a possible eruption forecasting tool, *Science*, **306**, 1543–1546.
- Haeussler, P.J., Bruhn, R.L. & Pratt, T.L., 2000. Potential seismic hazards and tectonics of the upper Cook Inlet basin, Alaska, based on analysis of Pliocene and younger deformation, *Geol. Soc. Am. Bull.*, **112**, 1414–1429.
- Haring, M.O., Schanz, U., Ladner, F. & Dyer, B.C., 2008. Characterisation of the Basel 1 enhanced geothermal system, *Geothermics*, **37**, 469–495.
- Horálek, J., Jechumtálová, Z., Dorbath, L., Šílený, J., 2010. Source mechanisms of micro-earthquakes induced in a fluid injection experiment at the HDR site Soultz-sous-Forêts (Alsace) in 2003 and their temporal and spatial variations, *Geophys. J. Int.*, **181**, 1547–1565.
- Jolly, A.D., Page, R.A. & Power, J.A., 1994. Seismicity and stress in the vicinity of Mount Spurr volcano, south central Alaska, *J. geophys. Res.*, **99**, 15 305–15 318.
- Jolly, A.D. *et al.* 2001. Catalog of earthquake hypocenters at Alaskan Volcanoes: January 1, 1994 through December 31, 1999, *U.S. Geol. Surv. Open-File Rep.*, **01–189**, 90pp.
- Kissling, E., Ellsworth, W.L., Eberhart-Phillips, D. & Kadolfer, U., 1994. Initial reference models in local earthquake tomography, *J. geophys. Res.*, **99**, 19 635–19 646.
- Lu, Z., Wicks, C., Power, J.A. & Dzurisin, D., 2000. Ground deformation associated with the March 1996 earthquake swarm at Akutan Volcano, Alaska, revealed by satellite radar interferometry, *J. geophys. Res.*, **105**, 21 483–21 495.
- Lu, Z., Dzurisin, D., Wicks, C., Power, J., Kwoun, O. & Rykhus, R., 2007. Diverse deformation patterns of Aleutian volcanoes from satellite interferometric synthetic aperture radar (InSAR), *Geophys. Monogr. Ser.*, **172**, 249–261.
- McNutt, S.R. & Marzocchi, W., 2004. Simultaneous earthquake swarms and eruption in Alaska, Fall 1996: statistical significance and inference of a large aseismic slip event, *Bull. seism. Soc. Am.*, **94**, 1831–1841.
- Nye, C., Wyss, M., Ratchkovski, N. & Fletcher, H., 2002. Magmatism in the Denali Volcanic Gap, southern Alaska, *EOS, Trans. Am. geophys. Un.*, **83**(47), V12C-06.
- Ohta, Y., Freymuller, J.T., Hreinsdottir, S. & Suito, H., 2006. A large slow slip event and the depth of the seismogenic zone in the south central Alaska subduction zone. *Earth planet. Sci. Lett.*, **247**, 108–116.

- Pontoise, B. & Monfret, T., 2004. Shallow seismogenic zone detected from an offshore-onshore temporary seismic network in the Esmeraldas area (Northern Ecuador). *Geochem. Geophys. Geosyst.*, **5**, 1–22.
- Reasenber, P.A. & Oppenheimer, D.H., 1985. FPFIT, FPLOT and FPAGE: Fortran computer programs for calculating and displaying earthquake fault-plane solutions, *U.S. Geol. Surv. Open-File Rep.*, **1985–739**, 25pp.
- Roman, D.C. & Cashman, K.V., 2006. The origin of volcano-tectonic earthquake swarms, *Geology*, **35**, 457–460.
- Roman, D.C., Power, J.A., Moran, S.C., Cashman, K.V., Doukas, M.P., Neal, C.A. & Gerlach, T.M., 2004. Evidence for dike emplacement at Iliamna Volcano, Alaska in 1996, *J. Volc. Geotherm. Res.*, **130**, 265–284.
- Rondenay, S., Montesi, L.G.J. & Abers, G.A., 2010. New geophysical insight into the origin of the Denali volcanic gap. *Geophys. J. Int.*, **182**, 613–630.
- Ruppert, N.A., 2008. Stress map for Alaska from earthquake focal mechanisms, in *Geophys. Monogr. Ser.*, **179**, 351–367.
- Ruppert, N.A. & Hansen, R.A., 2010. Temporal and spatial variations of local magnitudes in Alaska and Aleutians and calibration with moment magnitudes. *Seismol. Res. Lett.*, **81**, 342.
- Sánchez, J.J., Wyss, M. & McNutt, S.R., 2004. Temporal-spatial variations of stress at Redoubt volcano, Alaska, inferred from inversion of fault-plane solutions, *J. Volc. Geotherm. Res.*, **130**, 1–30.
- Scholz, C.H., 2002. *The Mechanics of Earthquakes and Faulting*, 2nd edn, p.471, Cambridge University Press, Cambridge.
- Smith, K.D., Von Seggern, D.H., Blewitt, G., Preston, L.A., Anderson, J.G., Wernicke, B.P. & Davis, J.L., 2004. Evidence for deep magma injection beneath Lake Tahoe, Nevada-California, *Science*, **305**, 1277–1280.
- Smith, K., von Seggern, D.H., dePolo, D., Anderson, J.G., Biasi, G.P. & Anooshehpour, R., 2008. Seismicity of the 2008 Mogul-Somersett West Reno, Nevada earthquake sequence. *EOS, Trans. Am. geophys. Un.*, **89**(53), S53C-02.
- Sturm, M. & Benson, C.S., 1985. A history of jokulhlaups from Strandline Lake, Alaska, U.S.A., *J. Glaciol.*, **31**, 272–280.
- Toda, S., Stein, R.S. & Sagiya, T., 2002. Evidence from the AD 2000 Izu islands earthquake swarm that stressing rate governs seismicity, *Nature*, **419**, 58–61.
- Umakoshi, K., Shimizu, H. & Matsuwo, N., 2001. Volcano-tectonic seismicity at Unzen Volcano, Japan, 1985–1999, *J. Volc. Geotherm. Res.*, **112**, 117–131.
- Vidale, J.E., Boyle, K.L. & Shearer, P.M., 2006. Crustal earthquake bursts in California and Japan: their patterns and relation to volcanoes, *Geophys. Res. Lett.*, **33**, L20313, doi:10.1029/2006GL027723.
- Wiemer, S., Tytgat, G., Wyss, M. & Duenkel, U., 1999. Evidence for shear-wave anisotropy in the mantle wedge beneath south central Alaska, *Bull. seism. Soc. Am.*, **89**, 1313–1322.
- Wilson, F.H., Hults, C.P., Schmoll, H.R., Hauessler, P.J., Schmidt, J.M., Yehle, L.A. & Labay, K.A., 2009. Preliminary geologic map of the Cook Inlet region, Alaska, *U.S. Geol. Surv. Open-File Rep.*, **2009–1108**, 2pp.
- Wright, T.J., Ebinger, C., Biggs, J., Ayele, A., Yirgu, G., Keir, D. & Stork, A., 2006. Magma-maintained rift segmentation at continental rupture in the 2005 Afar dyking episode, *Nature*, **442**, 291–294.
- Yamashita, T., 1998. Simulation of seismicity due to fluid migration in a fault zone, *Geophys. J. Int.*, **132**, 674–686.